

# Unsupported $\mu$ -Oxo- and $\mu$ -Hydroxo-Iron(III) Dimers and Mononuclear Iron(III) Complexes with Pyridylbis(aminophenol) Ligands

Rajendra Shakya,<sup>[a]</sup> Douglas R. Powell,<sup>[a]</sup> and Robert P. Houser\*<sup>[a]</sup>

**Keywords:** Iron / N,O ligands / Bridging ligands / Bioinorganic chemistry

Unsupported hydroxo- and oxo-bridged diiron(III) and mononuclear iron(III) complexes with pyridylbis(aminophenol) ligands ( $L^{\text{amine}}2^-$  and  $(L^{\text{Bu-amine}})^{2-}$ ) were synthesized and characterized [ $H_2L^{\text{amine}} = 2,2'-(2\text{-methyl-2-(pyridin-2-yl)propane-1,3-diyl})\text{bis(azanediy)}\text{bis(methylene)diphenol}$ ;  $H_2L^{\text{Bu-amine}} = 6,6'-(2\text{-methyl-2-(pyridin-2-yl)propane-1,3-diyl})\text{bis(azanediy)}\text{bis(methylene)bis(2,4-di-tert-butylphenol)}$ ]. Dimeric  $[(FeL^{\text{amine}})_2(\mu\text{-OH})]BPh_4$  (**1**) and  $[(FeL^{\text{Bu-amine}})_2(\mu\text{-O})]$  (**2**), and monomeric  $[FeL^{\text{Bu-amine}}(OCH_3)]$  (**3**) were synthesized from ferric perchlorate. Monomeric  $[FeL^{\text{amine}}Cl]$  (**4**) and  $[FeL^{\text{Bu-amine}}Cl]$  (**5**) were synthesized from ferric chloride. Complex **1** is comprised of two  $[FeL^{\text{amine}}]^+$  units, where  $(L^{\text{amine}})^{2-}$  is pentadentate, bridged by a single hydroxo ligand. Intramolecular H-bonding between the NH groups on one  $[FeL^{\text{amine}}]^+$  unit and the phenolato O atoms of the other  $[FeL^{\text{amine}}]^+$  unit stabilizes the structure. Complex **2** is an oxo-bridged dimer, but the steric constraints from the *tert*-butyl

groups of  $(L^{\text{Bu-amine}})^{2-}$  prevent intramolecular H-bonding. Monomeric **4** and **5** are isostructural with pentadentate ligands  $(L^{\text{amine}})^{2-}$  or  $(L^{\text{Bu-amine}})^{2-}$ , respectively, and a chloro ligand in the sixth position of the six-coordinate iron(III) moieties. Conversion of **2** to its protonated hydroxo-bridged analog  $[(FeL^{\text{Bu-amine}})_2(\mu\text{-OH})]^+$  by treatment with mild acid was monitored spectroscopically and electrochemically, but the reaction was not reversible by treatment with base. Similarly, hydroxo-bridged **1** could not be deprotonated to generate its oxo-bridged analog,  $[(FeL^{\text{amine}})_2(\mu\text{-O})]$ , suggesting that the  $pK_a$  values of the hydroxo groups in **1** and  $[(FeL^{\text{Bu-amine}})_2(\mu\text{-OH})]^+$  are quite large. The CV of **2** revealed well-defined ligand-based redox couples, but no metal-based redox couples. When **2** was treated with mild acid, metal-based redox couples for  $[(FeL^{\text{Bu-amine}})_2(\mu\text{-OH})]^+$  grew in.

(© Wiley-VCH Verlag GmbH & Co. KGaA, 69451 Weinheim, Germany, 2009)

## Introduction

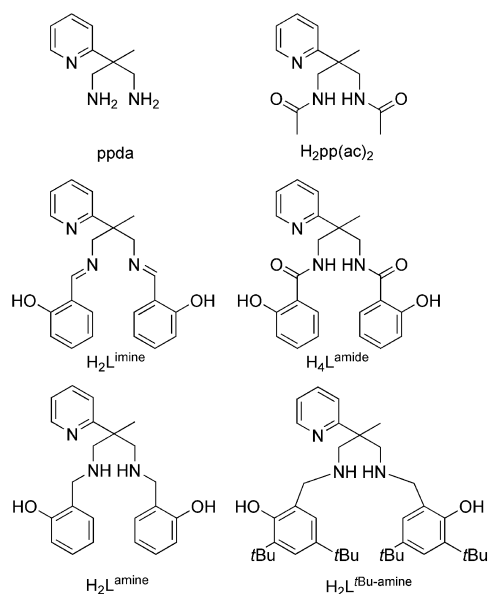
Oxo- and hydroxo-bridged binuclear iron complexes have been studied extensively due to their relevance to important metalloproteins and metalloenzymes including hemerythrin, methane monooxygenase (MMO), ribonucleotide reductase, and purple acid phosphatases, where the ubiquitous diiron motif in these enzymes is essential to their function.<sup>[1]</sup> Although the diiron moieties in these metalloproteins and metalloenzymes are often bridged by other bridging units, such as carboxylate groups from aspartate or glutamate amino acid side chains, unsupported hydroxo- or oxo-bridged species have been reported as possible intermediates in the hydroxylation mechanism of MMO based on related cytochrome P450 chemistry.<sup>[2]</sup> While there are a large number of structurally characterized unsupported oxo-bridged diiron complexes,<sup>[1a]</sup> to the best of our knowledge, only six unsupported hydroxo-bridged diiron complexes are known. Four of these are porphyrin species,<sup>[3]</sup>

and one is a non-heme diiron(II) complex with a tetrapodal polyamine ligand,  $pyN_4$ .<sup>[4]</sup> Only one of these is a non-heme diiron(III) complex,  $[(Fe(\text{salten}))_2(\mu\text{-OH})]BPh_4$ , where  $H_2\text{salten} = 4\text{-azaheptane-1,7-bis(salicylideneimine)}$ .<sup>[5]</sup> Here we report a new example of an unsupported hydroxo-bridged diiron(III) complex, where the ligand plays an important role in stabilizing this unusual structure, along with related oxo-bridged diiron(III) and mononuclear iron(III) complexes.

In our laboratory we have generated a series of pyridylamide ligands and studied the coordination chemistry of transition-metal complexes of various oxidation states and nuclearities.<sup>[6]</sup> We recently extended the pyridylamide family of ligands to a new family of ligands, including the pyridylbis(acetamide) ligand  $H_2pp(ac)_2$  (Scheme 1), that was found to support several novel mixed-valence copper complexes.<sup>[7]</sup> Most recently, we developed and synthesized three new ligands  $H_2L^{\text{imine}}$ ,  $H_2L^{\text{amine}}$ , and  $H_4L^{\text{amide}}$  (Scheme 1) that share a common backbone with  $H_2pp(ac)_2$  but contain phenol groups in place of the methyl in  $H_2pp(ac)_2$ , and were found to support copper(II) complexes of varying nuclearity.<sup>[8]</sup> Here we present two new iron(III) complexes with the previously reported  $H_2L^{\text{amine}}$  ligand, and three new iron(III) complexes with a new ligand,  $H_2L^{\text{Bu-amine}}$ .

[a] Department of Chemistry and Biochemistry, University of Oklahoma, Norman, Oklahoma, 73019, USA  
Fax: +1-405-325-6111  
E-mail: houser@ou.edu

Supporting information for this article is available on the WWW under <http://dx.doi.org/10.1002/ejic.200900794>.

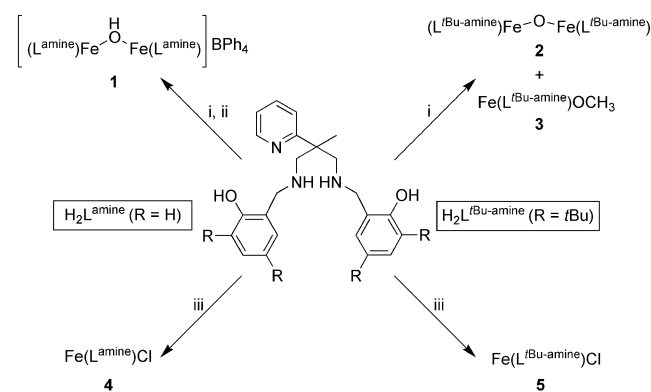


Scheme 1. Pyridylbis(amine), pyridylbis(imine), and pyridylbis(amide) ligands used in this study and related previous work.

## Results and Discussion

### Syntheses

The differences between  $H_2L^{\text{amine}}$  and  $H_2L^{\text{tBu-amine}}$  center on the substituents on the phenol rings (Scheme 1 and 2).  $H_2L^{\text{amine}}$  contains no substituents on the phenol rings, while  $H_2L^{\text{tBu-amine}}$  contains *tert*-butyl substituents in the 3- and 5-positions. Both  $H_2L^{\text{amine}}$  and  $H_2L^{\text{tBu-amine}}$  contain the same potential  $N_3O_2$  donor atom set, with pyridyl and amine N-donors, and when deprotonated, phenolate O-donors. While the unsubstituted ligand  $H_2L^{\text{amine}}$  was synthesized as reported previously from our laboratory,<sup>[8]</sup> the new ligand  $H_2L^{\text{tBu-amine}}$  was synthesized following a similar procedure by Schiff base condensation of 2-methyl-2-pyridine-2-ylpropane-1,3-diamine (ppda, Scheme 1)<sup>[9]</sup> with 3,5-di-*tert*-butylsalicylaldehyde, followed by reduction with  $NaBH_4$ .



Scheme 2. Structures of ligands  $H_2L^{\text{amine}}$  and  $H_2L^{\text{tBu-amine}}$  and the syntheses of 1–5. (i)  $Fe(ClO_4)_3 \cdot 6H_2O$ ,  $Et_3N$ ,  $CH_3OH$ . (ii)  $NaBPh_4$ ,  $CH_3OH$ . (iii)  $FeCl_3$ ,  $Et_3N$ ,  $CH_2Cl_2$ .

Using  $H_2L^{\text{amine}}$  and  $H_2L^{\text{tBu-amine}}$  we synthesized five new iron(III) complexes, including hydroxo- and oxo-bridged binuclear iron(III) complexes, and mononuclear iron(III) complexes. Ligand  $H_2L^{\text{amine}}$ , upon reacting with  $Fe(ClO_4)_3 \cdot 6H_2O$  in methanol in the presence of  $Et_3N$  to deprotonate the phenol group, produced a dark red solution from which a red powder was isolated by solvent evaporation. After counterion metathesis by treatment with  $NaBPh_4$ , X-ray quality crystals of the complex were isolated by solvent evaporation. The complex was formulated as the hydroxo-bridged species  $[(FeL^{\text{amine}})_2(\mu-OH)]BPh_4$  (**1**) by X-ray crystallography and elemental analysis. The ESI-MS peak at  $m/z = 879$  corresponds to the hydroxo-bridged diiron(III) cation, and a broad band at  $3420\text{ cm}^{-1}$  in the FTIR confirms the hydroxo group as the bridging unit.

Combining the *tert*-butyl-substituted ligand  $H_2L^{\text{tBu-amine}}$  with  $Fe(ClO_4)_3 \cdot 6H_2O$  and excess  $Et_3N$  in methanol at  $-20\text{ }^\circ\text{C}$  for ca. 24 h yielded a purple solution, which upon removal of solvent produced a dark purple powder. Crystallization by slow evaporation from a solution of 1:1 acetonitrile/hexanes yielded red crystals of  $[(FeL^{\text{tBu-amine}})_2(\mu-O)]$  (**2**) in poor yield. The absence of a strong band for the perchlorate anion at ca.  $1100\text{ cm}^{-1}$  in the FTIR spectrum of **2** combined with the ESI-MS peak envelope at  $m/z = 1328$  of a methanol solution of **2** indicated a diiron(III) species with a bridging oxo group. This synthetic procedure produced **2** as a minor product (30% yield), while the major product obtained was a dark blue powder which, upon characterization by FTIR spectroscopy, ESI-MS, and elemental analysis, was characterized as the mononuclear iron(III) methoxide species  $[FeL^{\text{tBu-amine}}(OCH_3)]$  (**3**).

The non-coordinating perchlorate anion and solvent choice are key to the syntheses of **1** and **2**, since using ferric chloride in dichloromethane instead of ferric perchlorate in methanol leads to simple iron(III) chloride monomers. The reaction of either  $H_2L^{\text{amine}}$  or  $H_2L^{\text{tBu-amine}}$  with anhydrous  $FeCl_3$  in dichloromethane using  $Et_3N$  to deprotonate the ligands yielded mononuclear complexes  $[FeL^{\text{amine}}Cl]$  (**4**) and  $[FeL^{\text{tBu-amine}}Cl] \cdot H_2O$  (**5**), respectively. Interestingly,  $FeCl_3$  with  $H_2L^{\text{tBu-amine}}$  and  $Et_3N$  in methanol produced **2**.

### X-ray Structures

Unlike the coordination behavior of  $(L^{\text{amine}})^{2-}$  and related ligand  $(L^{\text{imine}})^{2-}$  with copper(II) where the pyridyl group does not coordinate,<sup>[8]</sup> the pyridyl group coordinates to the iron centers in complexes 1–5, resulting six-coordinate complexes after the bridging O(H) group or the coordinating anion ( $Cl^-$  or  $CH_3O^-$ ) coordination is accounted for. The X-ray structure of **1** reveals that it consists of two  $Fe^{III}$  ions linked together by a single bridging hydroxo ligand and intramolecular H-bonding (Figure 1). Each  $Fe^{III}$  ion is coordinated in a distorted octahedral geometry, with the  $N_3O_2$  ligand donor atom set from the deprotonated pentadentate ligand  $(L^{\text{amine}})^{2-}$ , and a bridging hydroxo ligand rounding out the coordination environment. The overall +1 charge of the complex is balanced by one  $BPh_4^-$  counteranion.

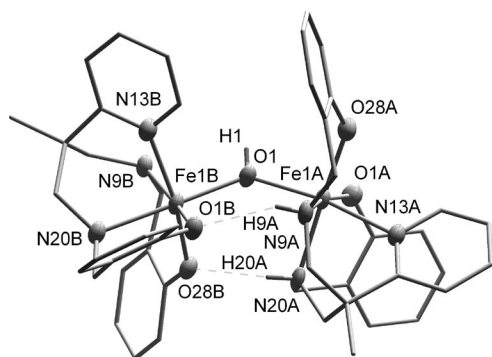


Figure 1. Representation of the X-ray structure of **1** with all H atoms except the N9A and N20A amine and  $\mu$ -hydroxo H atoms removed for clarity. Heteroatoms are shown with 50% probability thermal ellipsoids. H-bonding interactions are represented by dashed lines.

The coordination environments around Fe1A and Fe1B in **1**, while similar, are not the same. One iron center (Fe1A) has the pyridyl N atom (N13A) oriented *trans* to the bridging hydroxo ligand (O1), while the other iron atom (Fe1B) has one of the amine N atoms (N20B) *trans* to the bridging hydroxo ligand and the pyridyl N atom (N13B) is *cis*. The Fe–N bond length of the pyridyl N atom *trans* to the hydroxo group is slightly longer than the distance of the *cis* pyridyl N atom, 2.2119(19) Å vs. 2.151(2) Å, respectively. The bond lengths and angles involving the iron atoms (Table 1) are otherwise typical of six-coordinate Fe<sup>III</sup> species with similar ligands. While the coordination environment around the two iron centers in **1** closely resembles the only reported unsupported hydroxo-bridged non-heme diiron(III) complex, [(Fe(salten))<sub>2</sub>( $\mu$ -OH)]BPh<sub>4</sub>,<sup>[5]</sup> the key difference between these two compounds lies in their coordination modes. In the salten complex, the two [Fe(salten)]<sup>+</sup> units of the dimetallic cations are crystallographically equivalent and no H-bonding interactions exist between the two units, whereas in **1** the distance of one of the iron atoms from the bridging hydroxo oxygen is slightly longer than the other [Fe1A–O1, 2.0174(16) Å vs. Fe1B–O1, 2.0033(17) Å], and important H-bonding between each [FeL<sup>amine</sup>]<sup>+</sup> unit defines the structure.

The differences in coordination modes on each iron in **1** are a consequence of H-bonding interactions between the amine NH groups of one [FeL<sup>amine</sup>]<sup>+</sup> unit (N9A and N20A) with the phenolate O atoms of the other [FeL<sup>amine</sup>]<sup>+</sup> unit (O1B and O28B). The amine NH groups from the other ligand (N9B and N20B) are not involved in intra- or intermolecular H-bonding. The Fe–O(H)–Fe bond angle in **1** is 138.64(9)°, which is significantly smaller than the corresponding angle of 159.45(14)° in [(Fe(salten))<sub>2</sub>( $\mu$ -OH)]<sup>+</sup>. The Fe...Fe distance of 3.7616(7) Å in **1** is also shorter than the Fe...Fe distance of 3.928 Å in [(Fe(salten))<sub>2</sub>( $\mu$ -OH)]<sup>+</sup>.<sup>[5]</sup> The Fe–O(H)–Fe bond angle in **1** is also smaller than the Fe–O(H)–Fe bond angle of 146.7(2)° in the unsupported hydroxo-bridged non-heme diiron(II) complex with tetrapodal polyamine ligand pyN<sub>4</sub>.<sup>[4]</sup> These differences are likely a consequence of the H-bonding interactions pulling the

Table 1. Selected bond lengths [Å] and angles [°] for **1**.

Complex <b>1</b>			
Fe1A–O1	2.0174(16)	Fe1B–O1	2.0033(17)
Fe1A–O1A	1.9171(16)	Fe1B–O1B	1.9327(16)
Fe1A–O28A	1.9113(16)	Fe1B–O28B	1.9108(17)
Fe1A–N9A	2.160(2)	Fe1B–N9B	2.151(2)
Fe1A–N13A	2.2119(19)	Fe1B–N13B	2.177(2)
Fe1A–N20A	2.180(2)	Fe1B–N20B	2.169(2)
Fe1A...Fe1B	3.7616(7)		
O1–Fe1A–O1A	105.60(7)	O1–Fe1B–O1B	92.78(7)
O1–Fe1A–O28A	93.61(7)	O1–Fe1B–O28B	94.78(7)
O1–Fe1A–N9A	88.57(7)	O1–Fe1B–N9B	91.41(7)
O1–Fe1A–N20A	87.11(7)	O1–Fe1B–N13B	94.30(7)
O1A–Fe1A–O28A	90.40(7)	O1B–Fe1B–O28B	97.98(7)
O1A–Fe1A–N9A	90.62(7)	O1B–Fe1B–N9B	91.99(7)
O1A–Fe1A–N13A	88.46(7)	O1B–Fe1B–N20B	85.08(7)
O28A–Fe1A–N13A	92.82(7)	O28B–Fe1B–N13B	90.69(7)
O28A–Fe1A–N20A	91.80(7)	O28B–Fe1B–N20B	90.58(7)
N9A–Fe1A–N13A	84.66(7)	N9B–Fe1B–N13B	78.55(8)
N9A–Fe1A–N20A	86.64(8)	N9B–Fe1B–N20B	83.56(8)
N20A–Fe1A–N13A	78.57(7)	N20B–Fe1B–N13B	87.01(7)
O1–Fe1A–N13A	164.47(7)	O1–Fe1B–N20B	174.46(7)
O1A–Fe1A–N20A	166.93(7)	O1B–Fe1B–N13B	168.31(7)
O28A–Fe1A–N9A	177.25(7)	O28B–Fe1B–N9B	167.97(7)
Fe1B–O1–Fe1A	138.64(9)		

[FeL<sup>amine</sup>]<sup>+</sup> units together, a property not present in either of the reported unsupported hydroxo-bridged non-heme diiron complexes discussed above. In fact, the Fe–O(H)–Fe bond angle in **1** is closer to the Fe–O(H)–Fe bond angle of 123.1(2)° in the bis( $\mu$ -acetato)diiron(III) species [(FeTp)<sub>2</sub>( $\mu$ -OH)( $\mu$ -AcO)<sub>2</sub>], where Tp<sup>−</sup> is tris(pyrazolyl)hydroborate and AcO<sup>−</sup> is acetate.<sup>[10]</sup>

The structure of **2** is similar to **1** in that it consists of two [FeL<sup>tBu-amine</sup>]<sup>+</sup> units bridged, in this case, by an oxo ligand. Each Fe<sup>III</sup> is coordinated in a distorted octahedral geometry comprised of a N<sub>3</sub>O<sub>2</sub> ligand atom donor set from the deprotonated (L<sup>tBu-amine</sup>)<sup>2−</sup> ligands, and a single bridging oxo ligand in place of the hydroxo ligand in **1** (Figure 2). The Fe–N(py) bond lengths in **2** are slightly longer than the corresponding distances in **1**, possibly due to the stronger donating ability of the bridging oxo group compared to the hydroxo group (Table 2). The average Fe–O(phenolate) bond length of 1.962 Å in **2** is also slightly larger than the corresponding average bond length for **1**, which is 1.912 Å. Other bond lengths and angles involving the iron atoms in **2** are generally typical of Fe<sup>III</sup> complexes with similar ligands.

An important difference between **1** and **2** is that there is no H-bonding interactions between the (L<sup>tBu-amine</sup>)<sup>2−</sup> ligands in **2**. The pyridyl groups in both of the [FeL<sup>tBu-amine</sup>]<sup>+</sup> units of **2** are oriented *trans* to the bridging oxo group, which orients the phenolate O atoms such that they are not available for H-bonding. Stated another way, in order for the phenolate O atoms to be able to form H-bonds with the amine NH groups from the adjacent ligand, the ligand must be coordinated with an amine group *trans* to the bridging ligand, a condition that is not met in **2**.

As a result of the absence of any H-bonding between [FeL<sup>tBu-amine</sup>]<sup>+</sup> units in **2**, the Fe–O–Fe bond angle of 169.4(6)° is much larger than the corresponding Fe–O(H)–

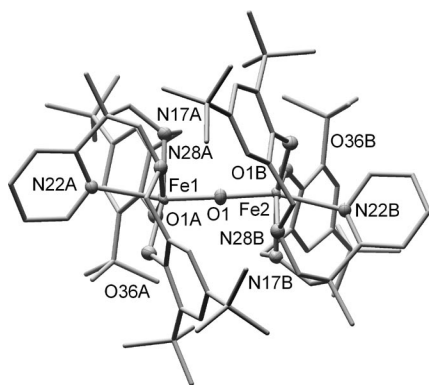


Figure 2. Representation of the X-ray structure of **2** with all H atoms removed for clarity. Heteroatoms are shown with 50% probability thermal ellipsoids.

Table 2. Selected bond lengths [Å] and angles [°] for **2**.

Complex <b>2</b>			
Fe1–O1	1.844(10)	Fe2–O1	1.793(10)
Fe1–O1A	1.963(9)	Fe2–O1B	1.971(9)
Fe1–O36A	1.962(10)	Fe2–O36B	1.954(10)
Fe1–N17A	2.155(12)	Fe2–N17B	2.163(12)
Fe1–N22A	2.334(12)	Fe2–N22B	2.261(12)
Fe1–N28A	2.243(12)	Fe2–N28B	2.251(12)
Fe1...Fe2	3.621(4)		
O1–Fe1–O1A	103.4(4)	O1–Fe2–O1B	104.5(4)
O1–Fe1–O36A	102.5(4)	O1–Fe2–O36B	103.3(4)
O1–Fe1–N17A	88.3(4)	O1–Fe2–N17B	88.4(5)
O1–Fe1–N28A	85.6(4)	O1–Fe2–N28B	85.5(4)
O1A–Fe1–N17A	89.4(4)	O1B–Fe2–N17B	90.2(4)
O1A–Fe1–N22A	92.2(4)	O1B–Fe2–N22B	92.4(4)
O36A–Fe1–O1A	98.7(4)	O36B–Fe2–O1B	96.9(4)
O36A–Fe1–N22A	82.8(4)	O36B–Fe2–N22B	85.1(4)
O36A–Fe1–N28A	90.2(4)	O36B–Fe2–N28B	90.0(4)
N17A–Fe1–N22A	83.8(4)	N17B–Fe2–N22B	80.6(4)
N17A–Fe1–N28A	79.4(4)	N17B–Fe2–N28B	80.4(4)
N28A–Fe1–N22A	77.6(4)	N28B–Fe2–N22B	76.2(4)
O1–Fe1–N22A	162.4(4)	O1–Fe2–N22B	159.9(4)
O1A–Fe1–N28A	165.5(4)	O1B–Fe2–N28B	166.2(4)
O36A–Fe1–N17A	164.5(4)	O36B–Fe2–N17B	164.3(4)
Fe1–O1–Fe2	169.4(6)		

Fe angle of 138.64(9)° in **1**. However, this bond angle is smaller than the linear bond angle of 180°, which is seen in many unsupported oxo-bridged diiron(III) complexes,<sup>[1a]</sup> but significantly larger than the Fe–O–Fe bond angle of 144.5(2)° observed in [(Fe(cbpN))<sub>2</sub>(μ-O)] where cbpN is a hydroxy-benzophenone-substituted triazacyclononane ligand that shares a N<sub>3</sub>O<sub>2</sub> donor set similar to (L<sup>tBu-amine</sup>)<sup>2-</sup>.<sup>[11]</sup> The near-linear Fe–O–Fe bond angle in **2** is likely due to the steric constraints imposed by the bulky *tert*-butyl groups on (L<sup>tBu-amine</sup>)<sup>2-</sup> combined with the absence of any H-bonding that could pull the [FeL<sup>tBu-amine</sup>]<sup>+</sup> units together. The Fe–O(oxo) distances in **2** of 1.844(10) Å and 1.793(10) Å are shorter than the Fe–O(H) distances in **1**, but longer than the Fe–O(oxo) distances found in unsupported μ-oxo-bridged diiron complexes reported in the literature [average Fe–O(oxo) 1.774 Å].<sup>[1a]</sup> However, one of the Fe–O(oxo) distances in **2** is even longer than the 1.807 Å Fe–O(oxo) dis-

tances in [(Fe(cbpN))<sub>2</sub>(μ-O)].<sup>[11]</sup> The Fe...Fe distance of 3.621(4) Å in **2** is shorter than the corresponding distance in **1**, due to the shorter Fe–O(oxo) distances in **2**.

The structures of **4** and **5** are similar, consisting of two monomers connected by H-bonding. Each monomer in **4** and **5** is comprised of an Fe<sup>III</sup> ion in a distorted octahedral geometry from the N<sub>3</sub>O<sub>2</sub> ligand donor atom set, and a Cl<sup>-</sup> ligand. The crystal structures and selected bond lengths and angles for complexes **4** and **5** are shown in Figures 3 and 4, respectively. The bond lengths angles around the iron atoms in both **4** and **5** are typical of six-coordinate, high spin Fe<sup>III</sup> complexes.<sup>[12]</sup> The X-ray structure of **4** consists of two symmetrically unrelated units connected by H-bonding between the amine NH groups from one monomer and the phenolate O atoms from the other (Figure 3). The H-bonding in **4** is reminiscent of the H-bonding observed in **1**, not surprising in light of the fact that they both contain ligand (L<sup>amine</sup>)<sup>2-</sup>.

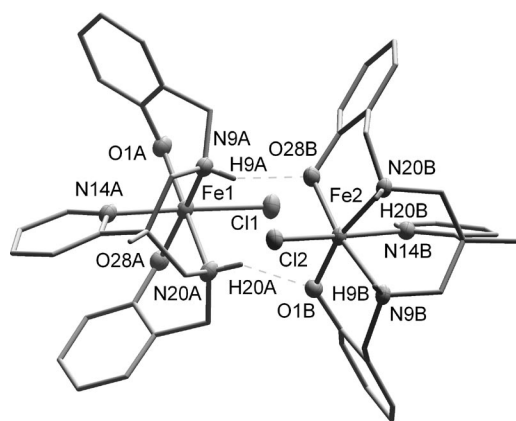


Figure 3. Representation of the X-ray structure of **4** with all H atoms except amine H atoms removed for clarity. Heteroatoms are shown with 50% probability thermal ellipsoids. H-bonding interactions are represented by dashed lines.

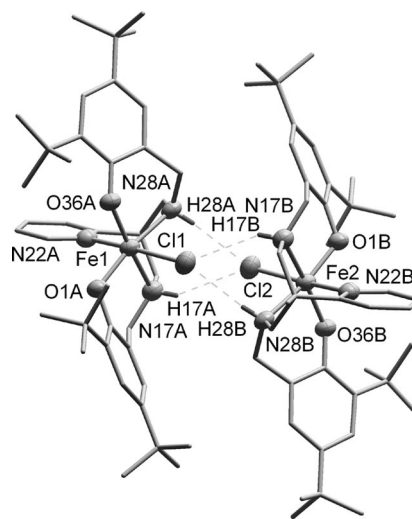


Figure 4. Representation of the X-ray structure of **5** with all H atoms except amine protons removed for clarity. Heteroatoms are shown with 50% probability thermal ellipsoids. H-bonding interactions are represented by dashed lines.

Table 3. Selected bond lengths [Å] and angles [°] for **4**.

Complex <b>4</b>			
Fe1–O1A	1.925(2)	Fe2–O1B	1.943(2)
Fe1–O28A	1.926(2)	Fe2–O28B	1.922(2)
Fe1–N9A	2.176(2)	Fe2–N9B	2.202(3)
Fe1–N14A	2.175(2)	Fe2–N14B	2.203(3)
Fe1–N20A	2.187(3)	Fe2–N20B	2.171(3)
Fe1–Cl1	2.3598(9)	Fe2–Cl2	2.3386(9)
O1A–Fe1–O28A	97.40(9)	O1B–Fe2–O28B	100.48(9)
O1A–Fe1–N14A	87.67(9)	O1B–Fe2–N14B	85.31(9)
O1A–Fe1–N9A	92.31(9)	O1B–Fe2–N9B	89.64(9)
O1A–Fe1–Cl1	95.79(7)	O1B–Fe2–Cl2	98.78(7)
O28A–Fe1–N14A	86.90(9)	O28B–Fe2–N14B	86.90(10)
O28A–Fe1–N20A	90.38(9)	O28B–Fe2–N20B	91.43(10)
O28A–Fe1–Cl1	100.14(6)	O28B–Fe2–Cl2	97.92(7)
N9A–Fe1–N14A	84.49(9)	N9B–Fe2–N14B	87.56(10)
N9A–Fe1–N20A	78.96(9)	N9B–Fe2–N20B	77.40(10)
N9A–Fe1–Cl1	87.78(7)	N9B–Fe2–Cl2	86.73(7)
N14A–Fe1–N20A	85.69(10)	N20B–Fe2–N14B	83.63(10)
N20A–Fe1–Cl1	89.75(7)	N20B–Fe2–Cl2	91.09(7)
O1A–Fe1–N20A	169.49(9)	O1B–Fe2–N20B	163.26(9)
O28A–Fe1–N9A	166.75(9)	O28B–Fe2–N9B	168.02(9)
N14A–Fe1–Cl1	171.65(7)	N14B–Fe2–Cl2	172.95(7)

Table 4. Selected bond lengths [Å] and angles [°] for **5**.

Complex <b>5</b>			
Fe1–O1A	1.8982(15)	Fe2–O1B	1.8986(16)
Fe1–O36A	1.9081(15)	Fe2–O36B	1.8936(16)
Fe1–N17A	2.231(2)	Fe2–N17B	2.171(2)
Fe1–N22A	2.189(2)	Fe2–N22B	2.171(2)
Fe1–N28A	2.172(2)	Fe2–N28B	2.240(2)
Fe1–Cl1	2.3766(8)	Fe2–Cl2	2.3568(9)
O1A–Fe1–O36A	100.42(6)	O1B–Fe2–O36B	99.67(7)
O1A–Fe1–N17A	90.37(7)	O1B–Fe2–N17B	89.84(7)
O1A–Fe1–N22A	91.49(7)	O1B–Fe2–N22B	93.65(7)
O1A–Fe1–Cl1	93.16(5)	O1B–Fe2–Cl2	97.42(5)
O36A–Fe1–N22A	91.47(7)	O36B–Fe2–N22B	90.41(7)
O36A–Fe1–N28A	90.30(7)	O36B–Fe2–N28B	89.89(7)
O36A–Fe1–Cl1	98.18(5)	O36B–Fe2–Cl2	93.98(5)
N17A–Fe1–N22A	78.80(7)	N17B–Fe2–N22B	87.47(8)
N28A–Fe1–N17A	79.00(7)	N17B–Fe2–N28B	80.49(7)
N17A–Fe1–Cl1	90.48(6)	N17B–Fe2–Cl2	86.22(6)
N28A–Fe1–N22A	87.87(7)	N22B–Fe2–N28B	78.85(8)
N28A–Fe1–Cl1	85.58(6)	N28B–Fe2–Cl2	89.16(6)
O1A–Fe1–N28A	169.28(7)	O1B–Fe2–N28B	167.95(7)
O36A–Fe1–N17A	165.71(7)	O36B–Fe2–N17B	170.38(7)
N22A–Fe1–Cl1	168.35(5)	N22B–Fe2–Cl2	167.23(5)

The structure of **5** consists of two six-coordinate monomers connected by weak H-bonding between the Cl<sup>−</sup> ligand and an NH group of one monomer with the corresponding groups from a second monomer (Figure 4). The N⋯Cl distances, which range from 3.214(2) Å to 3.368(2) Å, are typical of N–H⋯Cl hydrogen bonds.<sup>[13]</sup> The phenolate oxygen of one monomer is pointed away from the amine nitrogen of the other, probably due to the combined effects of steric hindrance of the *tert*-butyl groups and the symmetry of the pseudo inversion-related units. However, the coordination environment of the iron center in **5** is essentially the same as that seen in **4**.

### Spectroscopic Properties

Complexes **1–5** all exhibit strong bands in the near UV-region and less intense bands in the visible region (see Fig-

ure S1, Supporting Information). All the bands of binuclear complexes **1** and **2** are more intense than those of the mononuclear complexes **3–5**. The absorption bands observed in the near-UV region (below 300 nm) are assigned as  $\pi$ – $\pi^*$  transitions involving the aromatic units.<sup>[12]</sup> There is also an intense high energy band in the 300–400 nm region assigned to  $\pi$ – $d\sigma^*$  charge-transfer transitions.<sup>[14]</sup> However, these charge-transfer bands in binuclear complexes **1** and **2** appear only as shoulders. Based on an explanation proposed by Reem et al.,<sup>[15]</sup> the absorption bands in the oxo dimer region (300–400 nm) for the binuclear complexes are related to the bridging angles. For the bent Fe–O–Fe geometries in **1** and **2**, the peaks below 300 nm are assigned as the highest energy  $\pi$ -derived transitions, and the other lower energy transitions are assigned to the oxo- $p_z$ –Fe- $d_{xz}$  CT transitions. Complexes **1–5** also possess spectral features in the lower energy region (400–600 nm). For **1** and **2**, the low energy band is assigned as a hydroxo/oxo-to-iron(III) LMCT band, and the high intensity of this band overlaps with a band due to a phenolate-to-iron(III) LMCT. For the mononuclear complexes **3–5**, this low energy band is solely attributed to a  $\pi$ – $d\pi^*$  phenolate-to-iron(III) LMCT band. In **1** and **2**, the bridging oxo and hydroxo groups significantly influence the position of the low-energy LMCT transitions.<sup>[16]</sup> While the position of this LMCT band in **1** is at 520 nm ( $\epsilon = 6,600 \text{ M}^{-1} \text{ cm}^{-1}$ ), in **2** it is blue-shifted to 446 nm ( $\epsilon = 6,700 \text{ M}^{-1} \text{ cm}^{-1}$ ), which may be partly due to the stronger  $\pi$ -donating ability of the oxo bridge in **2** compared to the hydroxo bridge in **1**.<sup>[17]</sup>

The transformation of an oxo- to a hydroxo-bridged system is considered obligatory in heme-copper oxidases,<sup>[18]</sup> and such transformations have also been considered as a part of the oxygen binding process in hemerythrin.<sup>[19]</sup> The protonation of the oxo group upon treatment with HClO<sub>4</sub> has been observed in various heme<sup>[3a,3c]</sup> and non-heme<sup>[10]</sup> oxo-bridged diiron model compounds. Structurally, the protonation of the oxo group rehybridizes the bridging oxygen atom and the Fe–O–Fe unit becomes more bent along with significantly longer Fe–O bond lengths.

To explore the possible transformation of **2** to [(FeL<sup>*t*Bu-amine</sup>)<sub>2</sub>( $\mu$ -OH)]<sup>+</sup> by protonating the oxo bridging group, we examined the UV/Vis spectra of **2** after titration with acid. Dichloromethane solutions of **2** were titrated with  $8 \times 10^{-5} \text{ M}$  HClO<sub>4</sub>, also in dichloromethane, and followed by UV/Vis spectroscopy (Figure 5). After one equivalent of acid had been added, the low-energy LMCT transition is red-shifted from 446 nm to 520 nm, suggesting the protonation of the oxo group into a hydroxo group to form [(FeL<sup>*t*Bu-amine</sup>)<sub>2</sub>( $\mu$ -OH)]<sup>+</sup>. Back-titrating with base caused the transition at 520 nm to shift toward higher energy, but it was not possible to regenerate the spectrum of **2**. Hydroxo-bridged dimer **1** was treated with base to attempt to generate the oxo-bridged species [(FeL<sup>*t*Bu-amine</sup>)<sub>2</sub>( $\mu$ -O)]. The transition associated with the hydroxo group at 516 nm was blue-shifted upon addition of base (Et<sub>3</sub>N or proton sponge), but like the back titration of [(FeL<sup>*t*Bu-amine</sup>)<sub>2</sub>( $\mu$ -OH)]<sup>+</sup>, the amount of the blue-shift was less than expected. It is likely that the pK<sub>a</sub> of the hydroxo groups in **1** and [(FeL<sup>*t*Bu-amine</sup>)<sub>2</sub>-

$(\mu\text{-OH})^+$  are fairly high, thus requiring a much stronger base to deprotonate all of the hydroxo species.

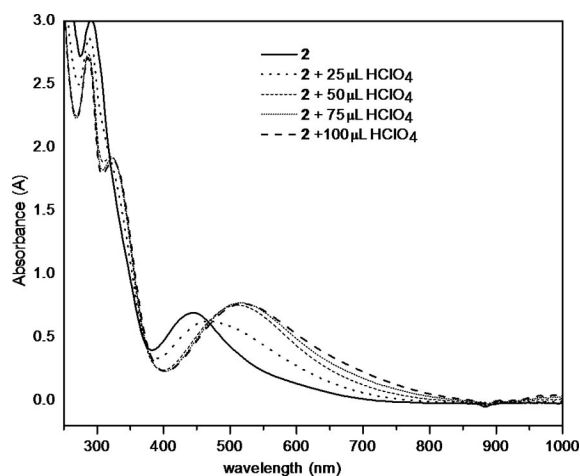


Figure 5. Titration of 0.10 mM  $\text{CH}_2\text{Cl}_2$  solution of **2** with a 0.08 mM  $\text{CH}_2\text{Cl}_2$  solution of  $\text{HClO}_4$  added via syringe in the volumes indicated.

The conversion of mononuclear complex **4** to the corresponding hydroxo-bridged diiron(III) species **1** was also probed by titration experiments followed by UV/Vis spectroscopy. Dichloromethane solutions of **4** were titrated with  $\text{Et}_3\text{N}$ , and dichloromethane solutions of **1** were titrated with acid ( $\text{HCl}$ ). The titration experiment carried out on **1** and **4** revealed that under the appropriate pH conditions, mononuclear complex **4** can be reversibly converted into the corresponding binuclear **1**. When **4** was titrated with  $\text{Et}_3\text{N}$ , the position of the low energy LMCT band was shifted from 520 nm to 486 nm, which is the same energy as that of the hydroxide-bridged diiron complex **1**, suggesting the conversion of **4** to **1**. Likewise, when **1** was titrated with  $\text{HCl}$ , the position of the low energy LMCT band was red-shifted to 520 nm, indicating the conversion of **1** to **4** (Figure S2).

### Electrochemistry

The redox behavior of complexes **1**–**5** were studied by cyclic voltammetry in dichloromethane. The cyclic voltammogram (CV) of **1** (Figure 6, dashed trace) exhibits two quasi-reversible redox waves centered at  $E_{1/2} = -630$  mV ( $\Delta E = 120$  mV) and  $-1190$  mV ( $\Delta E = 165$  mV) vs.  $\text{Ag}/\text{AgCl}$ . These peaks are believed to correspond to the  $\text{Fe}^{\text{III}}\text{Fe}^{\text{III}}/\text{Fe}^{\text{III}}\text{Fe}^{\text{II}}$  and  $\text{Fe}^{\text{III}}\text{Fe}^{\text{II}}/\text{Fe}^{\text{II}}\text{Fe}^{\text{II}}$  couples, respectively. In the positive potential range, there is an irreversible electrochemical wave at  $+830$  mV vs.  $\text{Ag}/\text{AgCl}$  assigned to ligand oxidation. The CV of related  $L^{\text{amine}}$  monomer **4** (Figure S3) has a single quasi-reversible feature centered at  $-450$  mV corresponding to the  $\text{Fe}^{\text{III}}/\text{Fe}^{\text{II}}$  redox couple, and an irreversible wave at  $+1200$  mV corresponding to ligand oxidation.

Interestingly, in contrast to similar oxo-bridged complexes with the TPA series of ligands [TPA = tris(2-pyridylmethyl)amine],<sup>[20]</sup> no metal-centered redox waves were observed for **2** from 0 to  $-1.8$  V (Figure 6, solid trace) at all

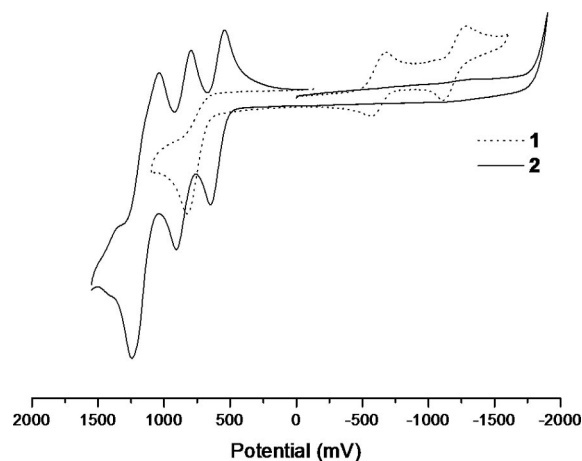


Figure 6. Cyclic voltammograms of complexes **1** (dashed line) and **2** (solid line) vs.  $\text{Ag}/\text{AgCl}$ , sample concentration ca. 1.0 mM in  $\text{CH}_2\text{Cl}_2$ , scan rate  $150$  mV  $\text{s}^{-1}$ ; 0.1 M TBAH supporting electrolyte.

scan rates. This suggests a very stable  $\text{Fe}^{\text{III}}$  oxidation state in **2**. However, in the positive potential range, **2** exhibits two quasi-reversible one-electron redox couples at 550 mV ( $\Delta E = 130$  mV) and 825 mV ( $\Delta E = 156$  mV), and an irreversible feature, possibly involving a two-electron oxidation, centered at 1086 mV ( $\Delta E = 270$  mV) vs.  $\text{Ag}/\text{AgCl}$ . These features are attributed to the oxidation of the phenolate groups leading to formation of phenoxyl radical species based on similarities to phenoxyl radicals and transition-metal complexes of phenoxyl radicals reported in the literature.<sup>[21]</sup> However, metal-centered redox features do appear in the CVs of related  $L^{\text{Bu-amine}}$  monomers **3** and **5** (Figures S4 and S5). **3** and **5** both exhibit one quasi-reversible feature corresponding to the  $\text{Fe}^{\text{III}}/\text{Fe}^{\text{II}}$  redox couple at  $-830$  mV and  $-670$  mV, respectively, and two quasi-reversible couples in the  $+800$  to  $+1200$  mV range corresponding to ligand oxidation. These observations suggest that factor(s) that lead to the absence of metal-centered redox features in the dimeric oxo-bridged **2** are not present in monomeric species **3** and **5**, despite containing the same ligand.

In order to further explore the protonation of the bridging oxo group, dichloromethane solutions of **2** were treated with varying amounts of  $8 \times 10^{-5}$  M  $\text{HClO}_4$ , and their CVs were recorded. The CVs recorded after treatment of **2** with 25 and 50  $\mu\text{L}$  of the  $\text{HClO}_4$  solution revealed the appearance of two irreversible redox waves centered at  $-640$  mV and  $-1300$  mV (Figure 7), which are similar to the redox waves observed for the metal-centered processes in hydroxo-bridged binuclear complex **1**. The ligand-centered redox processes observed in **2** were unaffected by the addition of  $\text{HClO}_4$ , suggesting the bridging oxo group in **2** is being protonated to a hydroxo-bridged species. The higher redox potentials of these newly appeared redox features compared to the redox potentials of the metal-centered processes in **1** are likely due to the *tert*-butyl substituents in **2**. Upon increasing the amount of  $\text{HClO}_4$ , the intensity of the metal-centered redox processes increases, but some of the ligand-centered processes disappear, probably due to decomposition of the binuclear species upon protonation of the phe-

nolate O atoms. These electrochemical observations corroborate the protonation of the bridging oxo group observed in the UV/Vis experiment.

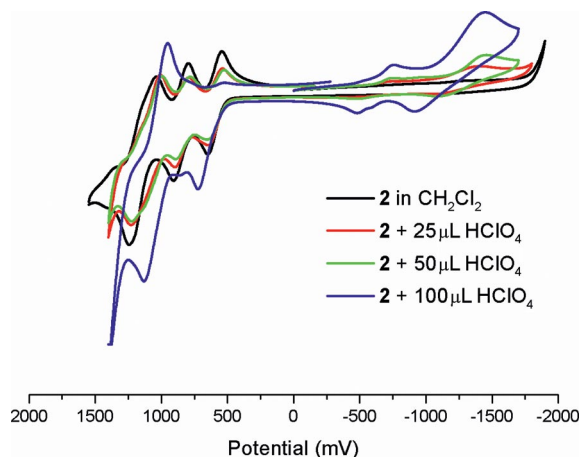


Figure 7. Cyclic voltammograms of complex **2** vs. Ag/AgCl with varying amounts of 0.08 mM HClO<sub>4</sub> in methanol added, sample concentration ca. 1 mM in CH<sub>2</sub>Cl<sub>2</sub>, scan rate 150 mV s<sup>-1</sup>; 0.1 M TBAH supporting electrolyte.

## Conclusions

In summary, iron(III) complexes of pyridylbis(aminophenol) ligands (L<sup>amine</sup>)<sup>2-</sup> and (L<sup>*t*Bu-amine</sup>)<sup>2-</sup> were synthesized and characterized. Iron dimers [(FeL<sup>amine</sup>)<sub>2</sub>(μ-OH)]·BPh<sub>4</sub> (**1**) and [(FeL<sup>*t*Bu-amine</sup>)<sub>2</sub>(μ-O)] (**2**), and monomer [FeL<sup>*t*Bu-amine</sup>(OCH<sub>3</sub>)] (**3**) were synthesized from ferric perchlorate, while monomers [FeL<sup>amine</sup>Cl] (**4**) and [FeL<sup>*t*Bu-amine</sup>Cl] (**5**) were synthesized from ferric chloride. Iron(III) dimers **1** and **2** are examples of unsupported O(H)-bridged diiron species, where no other bridging atoms support the structures. While this is not unusual for oxo-bridged diiron(III) complexes,<sup>[1a]</sup> **1** is a rare example of unsupported hydroxo-bridged diiron species,<sup>[3–5]</sup> being only the second example of a non-heme diiron(III) complex with an unsupported μ-OH ligand. The unique intramolecular H-bonding in **1** between the amine NH groups of one [FeL<sup>amine</sup>]<sup>+</sup> unit with the phenolato O atoms on the other [FeL<sup>amine</sup>]<sup>+</sup> supports the μ-OH group and stabilizes the structure of **1**. In contrast, steric constraints introduced by the *tert*-butyl groups in the [FeL<sup>*t*Bu-amine</sup>]<sup>+</sup> units of **2** orient the ligands such that intramolecular H-bonding is not possible.

The conversion of oxo-bridged **2** to its protonated hydroxo-bridged analog [(FeL<sup>*t*Bu-amine</sup>)<sub>2</sub>(μ-OH)]<sup>+</sup> by treatment with mild acid was monitored spectroscopically and electrochemically. However, the reaction was not reversible under the conditions tested, where solutions of [(FeL<sup>*t*Bu-amine</sup>)<sub>2</sub>(μ-OH)]<sup>+</sup> were treated with base to try to regenerate **2**. Similarly, hydroxo-bridged **1** could not be deprotonated to generate its oxo-bridged analog, [(FeL<sup>amine</sup>)<sub>2</sub>(μ-O)], suggesting that the pK<sub>a</sub> values of the hydroxo groups in **1** and [(FeL<sup>*t*Bu-amine</sup>)<sub>2</sub>(μ-OH)]<sup>+</sup> are quite large. Finally, the CV of **2** revealed well-defined ligand-based redox couples, but no metal-based redox couples. When the CVs of solutions of **2**

treated with mild acid were measured, metal-based redox couples grew in close to the potentials of the metal-based Fe<sup>III</sup>Fe<sup>III</sup>/Fe<sup>III</sup>Fe<sup>II</sup> and Fe<sup>III</sup>Fe<sup>II</sup>/Fe<sup>II</sup>Fe<sup>II</sup> couples observed for **1**. These observations suggest that the metal-based redox couples in **2** are outside of the potential range measured, making the iron(III) oxidation state in **2** extremely stable.

## Experimental Section

**General Procedures:** Unless otherwise stated, all reagents were used as received from commercial sources. The starting material for both of the ligands, 2-methyl-2-pyridin-2-ylpropane-1,3-diamine (ppda), was synthesized according to the literature procedure.<sup>[9]</sup> 2,2'-(2-Methyl-2-(pyridin-2-yl)propane-1,3-diyl)bis(azanediy)bis(methylene)diphenol (H<sub>2</sub>L<sup>amine</sup>) was synthesized according to our published procedure.<sup>[8]</sup> Solvents were doubly purified using alumina columns in a MBraun solvent purification system (MB-SPS). Infrared spectra were measured from 4000 to 400 cm<sup>-1</sup> as KBr pellets on a NEXUS 470 FTIR spectrometer. <sup>1</sup>H NMR spectra were measured using a Varian 300 MHz instrument. ESI-MS (positive) spectra were measured in Q-TOF quadrupole time-of-flight mass spectrometer (Micromass, Manchester, U. K.) containing a Z-spray electrospray ionization source (ESI). Elemental analyses were performed by Atlantic Microlabs, Norcross, GA. UV/Vis spectra were measured using a Shimadzu UV2401PC spectrophotometer in the range of 250 to 1000 nm. Cyclic voltammetry experiments were performed using a BAS 50W potentiometer. A standard three-electrode cell was employed with a glassy-carbon working electrode, a Pt-wire auxiliary electrode, and a Ag/AgCl reference electrode under an inert atmosphere at room temperature. X-Band EPR spectra were recorded for frozen CH<sub>2</sub>Cl<sub>2</sub> solutions of the complexes using a Bruker EMX spectrometer at 77 K. Solid state magnetic susceptibility was measured using a Johnson Matthey Magnetic Susceptibility Balance (MSB – AUTO) with a magnetic field strength of 4.5 kGauss and measurement range ± 1.999 × 10<sup>-4</sup> to ± 5 × 10<sup>-10</sup> cgs at 22 °C. A narrow bore sample tube with 0.400 cm outer diameter and 0.200 cm inner diameter was packed with sample to a minimum height of 15 mm. Solution magnetic susceptibilities of compounds **1**, **4**, and **5** in CD<sub>3</sub>CN and **2** in CDCl<sub>3</sub> were measured by Evans/NMR method.<sup>[22]</sup>

**Caution!** Perchlorate salts of metal complexes with organic ligands are potentially explosive. Although no difficulty was encountered during the syntheses, they should be prepared in small amounts and handled with caution.

**6,6'-[2-Methyl-2-(pyridin-2-yl)propane-1,3-diyl]bis(azanediy)bis(methylene)bis(2,4-di-*tert*-butylphenol) (H<sub>2</sub>L<sup>*t*Bu-amine</sup>):** H<sub>2</sub>L<sup>*t*Bu-amine</sup> was prepared by the condensation of 2-methyl-2-pyridin-2-ylpropane-1,3-diamine (0.82 g, 5.00 mmol) with 3,5-di-*tert*-butylsalicylaldehyde (2.34 g, 10.0 mmol) in 50 mL of CH<sub>3</sub>OH. The solution was stirred at 50 °C for 2 h, yielding a pale yellow solution. NaBH<sub>4</sub> (0.57 g, 15.0 mmol) was then added at 0 °C in small portions and the solution was stirred at room temperature for 2 h. The solvent was evaporated; the product was extracted with CH<sub>2</sub>Cl<sub>2</sub>, then dried with MgSO<sub>4</sub> and isolated after solvent evaporation (2.28 g, 76% yield). C<sub>39</sub>H<sub>59</sub>N<sub>3</sub>O<sub>2</sub>·CH<sub>3</sub>OH (633.49): calcd. C 75.78, H 10.02, N 6.63; found C 75.83, H 9.72, N 5.94. <sup>1</sup>H NMR (300 MHz, CDCl<sub>3</sub>, 293 K): δ = 1.28–1.48 (m, 39 H), 2.85–3.13 (m, 4 H), 3.89–3.91 (m, 4 H), 6.85–7.21 (m, 4 H), 7.30–7.70 (m, 3 H), 8.58 (d, *J* = 0.9 Hz, 1 H) ppm. FTIR (KBr): ν̄ = 3301 (O–H), 2956 (s, *t*Bu–CH), 2905 (s, *t*Bu–CH), 2867 (s, *t*Bu–CH) 1591 (s), 1480 (s), (C=N<sub>py</sub>,

C=C<sub>aromatic</sub>), 1390, 1361, 1301, 1236, 1203, 1165, 1124, 1092, 1026, 995, 925, 876, 821, 788, 748, 723, 672, 648, 542 cm<sup>-1</sup>. ESI-MS (CH<sub>3</sub>OH): *m/z* = 602 [H<sub>2</sub>L<sup>tBu-amine</sup> + H]<sup>+</sup>.

**[(FeL<sup>amine</sup>)<sub>2</sub>(μ-OH)]BPh<sub>4</sub> (1):** A 1 mL CH<sub>3</sub>OH solution of Fe(ClO<sub>4</sub>)<sub>3</sub>·6H<sub>2</sub>O (0.115 g, 0.250 mmol) was added dropwise to a 10 mL CH<sub>3</sub>OH solution of H<sub>2</sub>L<sup>amine</sup> (0.095 g, 0.25 mmol) and Et<sub>3</sub>N (0.07 mL, 0.5 mmol). The resulting dark red solution was stirred for 2 h at room temperature and filtered to discard any unreacted solids. A powder was isolated after removal of the solvent, was redissolved in CH<sub>3</sub>OH, and to this was added NaBPh<sub>4</sub> (0.13 g, 0.40 mmol) for counterion metathesis. The resulting solution was warmed to 50 °C for 2 h and then cooled down to room temperature. X-ray quality crystals were obtained by slow evaporation of the solvent (0.11 g, 70% yield). C<sub>72</sub>H<sub>83</sub>BF<sub>6</sub>N<sub>6</sub>O<sub>9</sub> (1298.50): calcd. C 66.57, H 6.44, N 6.47; found C 66.45, H 6.26, N 6.57. UV/Vis (CH<sub>2</sub>Cl<sub>2</sub>): λ<sub>max</sub> (ε, M<sup>-1</sup>cm<sup>-1</sup>) = 275 (23,100), 320 (10,200), 516 (6,580) nm. FTIR (KBr): ν̄ = 3420 (μ-OH), 3133, 3054, 2906, 1595 (s), 1570, 1479 (s, C=N<sub>py</sub>, C=C<sub>aromatic</sub>), 1455, 1427, 1389, 1268, 1150, 1112, 1064, 1031, 909, 881, 757, 732, 705, 613, 604, 510, 477 cm<sup>-1</sup>. ESI-MS (CH<sub>3</sub>OH): *m/z* = 431 [FeL<sup>amine</sup>]<sup>+</sup>, 879 [Fe(L<sup>amine</sup>)<sub>2</sub>(μ-OH)]<sup>+</sup>. EPR (9.457 GHz, mod. amp. 10.0 G, CH<sub>2</sub>Cl<sub>2</sub>, 77 K): *g* = 4.20 (strong) and *g* = 2.03 (weak). Solution magnetic moment (Evans method, 19.8 °C, 1.68 × 10<sup>-3</sup> M, [D<sub>3</sub>]acetonitrile): 2.64 μ<sub>B</sub>/Fe. Solid-state magnetic moment (MSB-Auto, 4.5 kG, 22.0 °C): 2.38 μ<sub>B</sub>/Fe.

**[(FeL<sup>tBu-amine</sup>)<sub>2</sub>(μ-O)] (2):** A 1 mL CH<sub>3</sub>OH solution of Fe(ClO<sub>4</sub>)<sub>3</sub>·6H<sub>2</sub>O (0.046 g, 0.10 mmol) was added dropwise to a 2 mL CH<sub>3</sub>OH solution of H<sub>2</sub>L<sup>tBu-amine</sup> (0.060 g, 0.10 mmol) and Et<sub>3</sub>N (0.06 mL, 0.45 mmol) at -20 °C. The resulting purple solution was stirred for 3 h at -20 °C and then stirred for another 16 h at room temperature. The solvent was removed under reduced pressure. X-ray quality crystals of **2** were obtained by slow evaporation of a 1:1 acetonitrile/hexane solution of the product mixture (0.020 g, 30% yield). C<sub>78</sub>H<sub>114</sub>Fe<sub>2</sub>N<sub>6</sub>O<sub>5</sub> (1326.75): calcd. C 70.57, H 8.66, N 6.33; found C 70.70, H 8.68, N 6.34. UV/Vis (CH<sub>2</sub>Cl<sub>2</sub>): λ<sub>max</sub> (ε, M<sup>-1</sup>cm<sup>-1</sup>) = 291 (28,500), 446 (6,720) nm. FTIR (KBr): ν̄ = 2953 (s, *t*Bu-CH), 2901 (s, *t*Bu-CH), 2866 (s, *t*Bu-CH), 1597 (s), 1573, 1467 (s, C=N<sub>py</sub>, C=C<sub>aromatic</sub>), 1439, 1412, 1391, 1361, 1300, 1268, 1239, 1203, 1167, 1090, 834, 745, 544, 477 cm<sup>-1</sup>. ESI-MS (CH<sub>3</sub>OH): *m/z* = 655 [FeL<sup>tBu-amine</sup>]<sup>+</sup>, 1328 [(Fe(L<sup>tBu-amine</sup>)<sub>2</sub>(μ-O)] + H)<sup>+</sup>. EPR (9.457 GHz, mod. amp. 10.0 G, CH<sub>2</sub>Cl<sub>2</sub>, 77 K): *g* = 4.21 (strong) and *g* = 2.02 (weak). Solution magnetic moment (Evans method, 19.8 °C, 9.30 × 10<sup>-3</sup> M, [D<sub>1</sub>]chloroform): 2.016 μ<sub>B</sub>/Fe. Solid-state magnetic moment (MSB-Auto, 4.5 kG, 22.0 °C): 1.919 μ<sub>B</sub>/Fe.

**[FeL<sup>tBu-amine</sup>(OCH<sub>3</sub>)] (3):** This complex is the major product in the synthesis of **2** (see above). A dark blue powder was isolated from the recrystallization mother liquor (after crystals of **2** were removed by decanting the solvent) by removal of solvent under vacuum. The powder was redissolved in dichloromethane, washed with water, and the organic layer was dried with anhydrous MgSO<sub>4</sub> and then filtered. A blue powder was isolated by removal of the solvent under vacuum (0.046 g, 60% yield). C<sub>40</sub>H<sub>60</sub>FeN<sub>3</sub>O<sub>3</sub>·CH<sub>2</sub>Cl<sub>2</sub> (770.35): calcd. C 63.81, H 8.10, N 5.45; found C 64.52, H 8.01, N 5.35. UV/Vis (CH<sub>2</sub>Cl<sub>2</sub>): λ<sub>max</sub> (ε, M<sup>-1</sup>cm<sup>-1</sup>) = 283 (9,850), 335 (5,610), 600 (3,100) nm. FTIR (KBr): ν̄ = 3257, 2953 (s, *t*Bu-CH), 2901 (s, *t*Bu-CH), 2866 (s, *t*Bu-CH), 1660, 1603 (s), 1562, 1466 (s, C=N<sub>py</sub>, C=C<sub>aromatic</sub>), 1439, 1412, 1361, 1300, 1267, 1240, 1203, 1168, 1107, 1018, 870, 834, 623, 546, 485 cm<sup>-1</sup>. ESI-MS (CH<sub>3</sub>OH): *m/z* = 655 [Fe(L<sup>tBu-amine</sup>)]<sup>+</sup>.

**[FeL<sup>amine</sup>Cl] (4):** Anhydrous FeCl<sub>3</sub> (0.0324 g, 0.200 mmol) was added to a 5 mL CH<sub>2</sub>Cl<sub>2</sub> solution of HL<sup>amine</sup> (0.076 g, 0.20 mmol) and Et<sub>3</sub>N (0.08 mL, 0.60 mmol). The resulting dark red solution

was stirred at room temperature for 2 h and then filtered to remove any unreacted solids. X-ray quality crystals were obtained from the solution after crystallization by slow evaporation of the solvent (0.065 g, 70% yield). C<sub>23</sub>H<sub>25</sub>ClFeN<sub>3</sub>O<sub>2</sub> (466.10): calcd. C 59.18, H 5.40, N 9.00; found C 59.34, H 5.79, N 8.56. UV/Vis (CH<sub>2</sub>Cl<sub>2</sub>): λ<sub>max</sub> (ε, M<sup>-1</sup>cm<sup>-1</sup>) = 277 (9,250), 318 (5,010), 519 (2,590) nm. FTIR (KBr): ν̄ = 3248, 1594 (s), 1569, 1478 (s, C=N<sub>py</sub>, C=C<sub>aromatic</sub>), 1453, 1398, 1384, 1273, 1172, 1062, 1037, 909, 820, 758, 609, 510, 474 cm<sup>-1</sup>. ESI-MS (CH<sub>3</sub>OH): *m/z* = 431 [Fe(L<sup>amine</sup>)]<sup>+</sup>. EPR (9.457 GHz, mod. amp. 10.0 G, CH<sub>2</sub>Cl<sub>2</sub>, 77 K): *g* = 9.24 (weak) and *g* = 4.18 (strong). Solution magnetic moment (Evans method, 19.8 °C, 1.68 × 10<sup>-2</sup> M, [D<sub>3</sub>]acetonitrile): 2.64 μ<sub>B</sub>/Fe. Solid-state magnetic moment (MSB-Auto, 4.5 kG, 22.0 °C): 2.82 μ<sub>B</sub>/Fe.

**[FeL<sup>tBu-amine</sup>Cl] (5):** Anhydrous FeCl<sub>3</sub> (0.0162 g, 0.100 mmol) was added to a 3 mL CH<sub>2</sub>Cl<sub>2</sub> solution of HL<sup>tBu-amine</sup> (0.060 g, 0.100 mmol) and Et<sub>3</sub>N (0.04 mL, 0.3 mmol). The resulting dark blue solution was stirred at room temperature for 2 h and then filtered to remove any unreacted solids. The blue powder was isolated from the reaction solution. X-ray quality crystals were obtained after recrystallization by slow evaporation of ethyl ether (0.052 g, 75% yield). Complex **5** is hygroscopic, and despite our efforts to dry it, water was always present in the elemental analysis. C<sub>39</sub>H<sub>57</sub>ClFeN<sub>3</sub>O<sub>2</sub>·H<sub>2</sub>O (708.36): calcd. C 66.05, H 8.39, N 5.92; found C 66.02, H 8.37, N 5.64. UV/Vis (CH<sub>2</sub>Cl<sub>2</sub>): λ<sub>max</sub> (ε, M<sup>-1</sup>cm<sup>-1</sup>) = 285 (12,700), 333 (6,630), 584 (3,100) nm. FTIR (KBr): ν̄ = 3217, 3175, 2951 (s, *t*Bu-CH), 2902 (s, *t*Bu-CH), 2864 (s, *t*Bu-CH), 1601 (s), 1562, 1466 (s, C=N<sub>py</sub>, C=C<sub>aromatic</sub>), 1438, 1412, 1390, 1360, 1299, 1266, 1240, 1203, 1168, 1075, 834, 544, 477 cm<sup>-1</sup>. ESI-MS (CH<sub>3</sub>OH): *m/z* = 655 [Fe(L<sup>tBu-amine</sup>)]<sup>+</sup>. EPR (9.457 GHz, mod. amp. 10.0 G, CH<sub>2</sub>Cl<sub>2</sub>, 77 K): *g* = 9.2 (weak) and *g* = 4.23 (strong). Solution magnetic moment (Evans method, 19.8 °C, 1.2 × 10<sup>-2</sup> M, [D<sub>3</sub>]acetonitrile): 3.068 μ<sub>B</sub>/Fe. Solid-state magnetic moment (MSB-Auto, 4.5 kG, 22.0 °C): 2.940 μ<sub>B</sub>/Fe.

**X-ray Crystal Structure Determination:** X-ray quality crystals of **1** were obtained by slow evaporation of a methanol solution of **1**. Single crystals of **2** were obtained by slow evaporation of a 1:1 acetonitrile/hexane solution of **2**. Single crystals of **4** and **5** were obtained by slow evaporation of methanol or ethyl ether solutions, respectively. Intensity data for all the compounds were collected using a diffractometer with a Bruker APEX ccd area detector<sup>[23]</sup> and graphite-monochromated Mo-K<sub>α</sub> radiation (λ = 0.71073 Å). The samples were cooled to 100(2) K. Cell parameters were determined from a non-linear least-squares fit of the data. The data were corrected for absorption by the semi-empirical method.<sup>[24]</sup> The structure was solved by direct methods and refined by full-matrix least-squares methods on *F*<sup>2</sup>.<sup>[25]</sup> Hydrogen atom positions of hydrogen atoms bonded to carbon atoms were initially determined by geometry and refined by a riding model. Hydrogen atoms bonded to nitrogen or oxygen atoms were located on a difference map, and their positions were refined independently. Non-hydrogen atoms were refined with anisotropic displacement parameters. Hydrogen atom displacement parameters were set to 1.2 (1.5 for methyl) times the displacement parameters of the bonded atoms. Crystal data for **1**·(CH<sub>4</sub>O)<sub>2</sub>·(H<sub>2</sub>O) and **2**·(C<sub>2</sub>H<sub>3</sub>N)<sub>5</sub> are summarized in Table 5, and crystal data for **4** and **5**·(C<sub>4</sub>H<sub>10</sub>O) are summarized in Table 6. Selected bond lengths and angles for **1–2** and **4–5** are summarized in Tables 1, 2, 3, and 4.

CCDC-736595 (for **1**·2CH<sub>4</sub>O·H<sub>2</sub>O), -736596 (for **2**·5C<sub>2</sub>H<sub>3</sub>N), -736597 (for **4**), -736598 (for **5**·C<sub>4</sub>H<sub>10</sub>O) contain the supplementary crystallographic data for this paper. These data can be obtained free of charge from The Cambridge Crystallographic Data Centre via www.ccdc.cam.ac.uk/data\_request/cif.

Table 5. Crystallographic data for complexes **1** and **2**.

	1·2CH <sub>4</sub> O·H <sub>2</sub> O	2·5C <sub>2</sub> H <sub>3</sub> N
Formula	C <sub>72</sub> H <sub>81</sub> BF <sub>2</sub> N <sub>6</sub> O <sub>8</sub>	C <sub>88</sub> H <sub>129</sub> Fe <sub>2</sub> N <sub>11</sub> O <sub>5</sub>
Fw	1280.94	1532.72
Space group	P $\bar{1}$	P2 <sub>1</sub> /n
a [Å]	11.448(2)	13.661(3)
b [Å]	15.643(4)	31.106(7)
c [Å]	19.253(4)	20.710(5)
$\alpha$ [°]	71.920(8)	90
$\beta$ [°]	88.393(7)	94.797(8)
$\gamma$ [°]	84.240(7)	90
V [Å <sup>3</sup> ]	3261.0(12)	8770(3)
Z	2	4
$\rho_{\text{calcd.}}$ [mg/m <sup>-3</sup> ]	1.305	1.161
$\mu$ [mm <sup>-1</sup> ]	0.506	0.385
$\theta$ [°]	1.38 to 26.00	2.08 to 18.00
R1 <sup>[a]</sup>	0.0453	0.1483
wR2 <sup>[b]</sup>	0.1292	0.3354
GOF on F <sup>2</sup>	1.051	1.174

[a]  $R1 = \Sigma \|F_o\| - |F_c| / \Sigma \|F_o\|$ . [b]  $wR2 = \{\Sigma [w(F_o^2 - F_c^2)^2] / \Sigma [w(F_o^2)^2]\}^{1/2}$ .

Table 6. Crystallographic data for complexes **4** and **5**.

	<b>4</b>	5·C <sub>4</sub> H <sub>10</sub> O
Formula	C <sub>23</sub> H <sub>25</sub> ClFeN <sub>3</sub> O <sub>2</sub>	C <sub>43</sub> H <sub>67</sub> ClFeN <sub>3</sub> O <sub>3</sub>
Fw	466.76	765.30
Space group	Cc	P $\bar{1}$
a [Å]	14.304(3)	13.737(3)
b [Å]	16.283(4)	14.409(3)
c [Å]	18.928(4)	23.904(5)
$\alpha$ [°]	90	89.985(5)
$\beta$ [°]	101.987(8)	81.727(5)
$\gamma$ [°]	90	67.005(6)
V [Å <sup>3</sup> ]	2807.8(16)	4302.0(16)
Z	8	4
$\rho_{\text{calcd.}}$ [mg/m <sup>-3</sup> ]	1.438	1.182
$\mu$ [mm <sup>-1</sup> ]	0.848	0.452
$\theta$ [°]	1.92 to 26.00	1.63 to 26.00
R1 <sup>[a]</sup>	0.0342	0.0456
wR2 <sup>[b]</sup>	0.0815	0.1155
GOF on F <sup>2</sup>	1.001	1.007

[a]  $R1 = \Sigma \|F_o\| - |F_c| / \Sigma \|F_o\|$ . [b]  $wR2 = \{\Sigma [w(F_o^2 - F_c^2)^2] / \Sigma [w(F_o^2)^2]\}^{1/2}$ .

**Supporting Information** (see also the footnote on the first page of this article): Crystallographic data in CIF format, UV/Vis spectra of complexes **1–5** (Figure S1), reversible conversion of **1** and **4** followed by UV/Vis spectroscopy (Figure S2), and cyclic voltammograms for **3–5** (Figures S3–S5).

## Acknowledgments

This work was supported by the National Science Foundation (NSF CHE-0616941). Additionally, we thank the NSF for the purchase of a CCD-equipped X-ray diffractometer (CHE-0130835) and Prof. Dr. A. Grohmann (Technische Universität Berlin) for fruitful discussions and the gift of several grams of 2-methyl-2-(2-pyridinyl)-1,3-propanediol.

[1] a) D. M. Kurtz, *Chem. Rev.* **1990**, *90*, 585; b) B. J. Wallar, J. D. Lipscomb, *Chem. Rev.* **1996**, *96*, 2625; c) E. I. Solomon, T. C. Brunold, M. I. Davis, J. N. Kemsley, S.-K. Lee, N. Lehnert, F. Neese, A. J. Skulan, Y.-S. Yang, J. Zhou, *Chem. Rev.* **2000**, *100*, 235.

- [2] M. Merckx, D. A. Kopp, M. H. Sazinsky, J. L. Blazyk, J. Muller, S. J. Lippard, *Angew. Chem. Int. Ed.* **2001**, *40*, 2782.
- [3] a) W. R. Scheidt, B. Cheng, M. K. Safo, F. Cukiernik, J. C. Marchon, P. G. Debrunner, *J. Am. Chem. Soc.* **1992**, *114*, 4420; b) C. H. Hung, W. C. Chen, G. H. Lee, S. M. Peng, *Chem. Commun.* **2002**, 1516; c) D. R. Evans, R. S. Mathur, K. Heerwegh, C. A. Reed, Z. W. Xie, *Angew. Chem. Int. Ed. Engl.* **1997**, *36*, 1335.
- [4] J. Pitarch López, H. Kampf, M. Grunert, P. Gutlich, F. W. Heinemann, R. Prakash, A. Grohmann, *Chem. Commun.* **2006**, 1718.
- [5] J. Jullien, G. Juhasz, P. Mialane, E. Dumas, C. R. Mayer, J. Marrot, E. Riviere, E. L. Bominaar, E. Munck, F. Secheresse, *Inorg. Chem.* **2006**, *45*, 6922.
- [6] a) U. Pal Chaudhuri, L. R. Whiteaker, A. Mondal, E. L. Klein, D. R. Powell, R. P. Houser, *Inorg. Chim. Acta* **2007**, *360*, 3610; b) L. Yang, R. P. Houser, *Inorg. Chem.* **2006**, *45*, 9416; c) A. Mondal, Y. Li, M. A. Khan, J. H. Ross, R. P. Houser, *Inorg. Chem.* **2004**, *43*, 7075; d) U. Pal Chaudhuri, L. R. Whiteaker, L. Yang, R. P. Houser, *Dalton Trans.* **2006**, 1902; e) E. L. Klein, M. A. Khan, R. P. Houser, *Inorg. Chem.* **2004**, *43*, 7272.
- [7] L. Yang, D. R. Powell, E. L. Klein, A. Grohmann, R. P. Houser, *Inorg. Chem.* **2007**, *46*, 6831.
- [8] R. Shakya, A. Jozwiuk, D. R. Powell, R. P. Houser, *Inorg. Chem.* **2009**, *48*, 4083.
- [9] S. Friedrich, M. Schubart, L. H. Gade, I. J. Scowen, A. J. Edwards, M. McPartlin, *Chem. Ber./Recl.* **1997**, *130*, 1751.
- [10] W. H. Armstrong, S. J. Lippard, *J. Am. Chem. Soc.* **1984**, *106*, 4632.
- [11] G. M. Mockler, J. Dejersey, B. Zerner, C. J. Oconnor, E. Sinn, *J. Am. Chem. Soc.* **1983**, *105*, 1891.
- [12] K. Hasan, C. Fowler, P. Kwong, A. K. Crane, J. L. Collins, C. M. Kozak, *Dalton Trans.* **2008**, 2991.
- [13] Y. R. Zhong, M. L. Cao, H. J. Mo, B. H. Ye, *Cryst. Growth Des.* **2008**, *8*, 2282.
- [14] J. W. Pyrz, A. L. Roe, L. J. Stern, L. Que, *J. Am. Chem. Soc.* **1985**, *107*, 614.
- [15] R. C. Reem, J. M. McCormick, D. E. Richardson, F. J. Devlin, P. J. Stephens, R. L. Musselman, E. I. Solomon, *J. Am. Chem. Soc.* **1989**, *111*, 4688.
- [16] X. Zhang, H. Furutachi, S. Fujinami, S. Nagatomo, Y. Maeda, Y. Watanabe, T. Kitagawa, M. Suzuki, *J. Am. Chem. Soc.* **2005**, *127*, 826.
- [17] A. J. Skulan, T. C. Brunold, J. Baldwin, L. Saleh, J. M. Bollinger, E. I. Solomon, *J. Am. Chem. Soc.* **2004**, *126*, 8842.
- [18] M. J. Scott, H. H. Zhang, S. C. Lee, B. Hedman, K. O. Hodgson, R. H. Holm, *J. Am. Chem. Soc.* **1995**, *117*, 568.
- [19] R. E. Stenkamp, L. C. Sieker, L. H. Jensen, J. D. McCallum, J. Sandersloehr, *Proc. Natl. Acad. Sci. USA* **1985**, *82*, 713.
- [20] R. C. Holz, T. E. Elgren, L. L. Pearce, J. H. Zhang, C. J. Oconnor, L. Que, *Inorg. Chem.* **1993**, *32*, 5844.
- [21] a) T. Storr, P. Verma, R. C. Pratt, E. C. Wasinger, Y. Shimazaki, T. D. P. Stack, *J. Am. Chem. Soc.* **2008**, *130*, 15448; b) L. Benisvy, A. J. Blake, D. Collison, E. S. Davies, C. D. Garner, E. J. L. McInnes, J. McMaster, G. Whittaker, C. Wilson, *Dalton Trans.* **2003**, 1975; c) T. Maki, Y. Araki, Y. Ishida, O. Onomura, Y. Matsumura, *J. Am. Chem. Soc.* **2001**, *123*, 3371.
- [22] D. F. Evans, *J. Chem. Soc.* **1959**, 2003.
- [23] a) *SMART, Software Reference Manual*, Bruker AXS, Madison, WI, USA, **1998**; b) *SAINTE Software Reference Manual*, Bruker AXS, Madison, WI, USA, **1998**.
- [24] G. M. Sheldrick, *SADABS, Program for empirical absorption correction of area detector data*, University of Göttingen, Germany, **2002**.
- [25] a) G. M. Sheldrick, *SHELXTL Version 6.10 Reference Manual*, Bruker AXS, Madison, Wisconsin, USA, **2000**; b) *International Tables for Crystallography*, vol. C, Kluwer, Boston, **1995**.

Received: August 14, 2009

Published Online: October 28, 2009